



1

2 **Brief communication: Unabated wastage of the Juneau and Stikine**
3 **icefields (southeast Alaska) in the early 21st century**

4 Etienne BERTHIER¹, Christopher LARSEN², William Durkin³, Michael Willis⁴, Matthew
5 Pritchard³

6 ¹LEGOS, Université de Toulouse, CNES, CNRS, IRD, UPS, F-31400 Toulouse, France

7 ²Geophysical Institute, University of Alaska Fairbanks, Fairbanks, Alaska, USA

8 ³Earth and Atmospheric Sciences Department, Cornell University, Ithaca, New York, USA

9 ⁴Cooperative Institute for Research in Environmental Sciences (CIRES), University of Colorado, Boulder, CO,
10 USA

11

12

13 *Correspondence to:* Etienne Berthier (etienne.berthier@legos.obs-mip.fr)

14 **Abstract.** The large Juneau and Stikine icefields (Alaska, JIF and SIF) lost mass rapidly in the second
15 part of the 20th century. Laser altimetry, gravimetry and sparse field measurements suggest continuing
16 mass loss in the early 21st century. However, two recent studies based on time series of SRTM and
17 ASTER digital elevation models (DEMs) indicate a slowdown in mass loss after 2000. Here, the
18 ASTER-based geodetic mass balance is recalculated, carefully avoiding the use of the SRTM DEM
19 because of the unknown penetration depth of the C-Band radar signal. We find strongly negative mass
20 balances from 2000 to 2016 (-0.68 ± 0.15 m w.e. a^{-1} for JIF and -0.83 ± 0.12 m w.e. a^{-1} for SIF), in
21 agreement with laser altimetry, confirming that mass losses are continuing at unabated rates for both
22 icefields. The SRTM DEM should be avoided or used very cautiously to estimate glacier volume
23 change, especially in the North Hemisphere and over timescales of less than ~ 20 yrs.

24 **1 Introduction**

25 The Juneau Icefield (JIF) and Stikine Icefield (SIF) are among the largest and southernmost icefields in
26 Alaska. The JIF covers about 3800 km² and the SIF close to 6000 km² at the border between
27 southeast Alaska and Canada (Kienholz et al., 2015). Together they account for roughly 10% of the
28 total glacierized area in Alaska. Both icefields experienced rapid mass loss in the second part of the
29 20th century (Arendt et al., 2002; Berthier et al., 2010; Larsen et al., 2007). Spaceborne gravimetry and
30 laser altimetry data suggest continuing rapid mass loss in southeast Alaska between 2003 and 2009
31 (Arendt et al., 2013).

32

33 For the JIF, Larsen et al. (2007) found a negative mass balance of -0.62 m w.e. a^{-1} for a time interval
34 starting in 1948/1982/1987 (depending on the map dates) and ending in 2000, the date of acquisition
35 of the shuttle radar topographic mission (SRTM) digital elevation model (DEM). Berthier et al. (2010)
36 found a slightly less negative multi-decadal mass balance (-0.53 ± 0.15 m w.e. a^{-1}) from the same
37 starting dates as Larsen et al. (2007) to a final DEM acquired in 2007. Repeat airborne laser altimetry



38 are available for nine glaciers of the JIF (Larsen et al., 2015) with a first survey performed in 1993 (2
39 glaciers), 1999 (1 glacier) and 2007 (6 glaciers). The last survey used in Larsen et al. (2015) was flown
40 in 2012 for all glaciers. During these varying time intervals, nine glaciers experienced strongly negative
41 mass balances (between -0.51 and -1.14 m w.e. a^{-1}) while Taku Glacier, which alone accounts for one
42 fifth of the JIF area, experienced a slightly positive mass balance ($+0.13$ m w.e. a^{-1}). Further, the
43 glaciological measurements performed on Lemon Creek Glacier (11.8 km² in 1998) suggest
44 accelerated mass loss since the mid-eighties: the glacier-wide mass balance declined from -0.30 m
45 w.e. a^{-1} during 1953-1985 to -0.60 m w.e. a^{-1} during 1986-2011 (Pelto et al., 2013). A modelling study
46 also found a negative mass balance for the entire JIF (-0.33 m w.e. a^{-1}) for 1971-2010 (Ziemen et al.,
47 2016). Their 40-year mass balance is a result of glacier mass stability until 1996 and rapid mass loss
48 afterwards. Taken together, all these studies point toward rapid mass loss of the JIF and accelerated
49 wastage during the last ~ 20 years. Conversely, a study based on the SRTM DEM and Advanced
50 Spaceborne Thermal Emission and Reflection Radiometer (ASTER) multi-temporal DEMs found a JIF
51 mass balance only moderately negative at -0.13 ± 0.12 m w.e. a^{-1} from 2000 to 2009/2013 (Melkonian
52 et al., 2014).

53

54 Only a few estimates of mass change are available on the larger and more remote SIF. Three of its
55 glaciers were surveyed with airborne laser altimetry from 1996 to 2013 and all experienced rapid mass
56 loss. The glacier-wide mass balances were -0.71 , -0.98 and -1.19 m w.e. a^{-1} for, respectively, Baird, Le
57 Conte and Triumph glaciers. Based on DEM differencing over several decades, Larsen et al. (2007)
58 and Berthier et al. (2010) found SIF-wide mass balance of, respectively, -1.48 and -0.76 ± 0.12 m w.e.
59 a^{-1} . A recent estimate based on the SRTM and ASTER DEMs suggest a less negative icefield-wide
60 mass balance of -0.57 ± 0.18 m w.e. a^{-1} from 2000 to 2014 (Melkonian et al., 2016).

61

62 If correct, Melkonian et al. (2014, 2016)'s estimates would imply a considerable slowdown of the mass
63 loss of the Juneau and, to a smaller extent, Stikine icefields during the first decade of the 21st century.
64 However, no clear trend in climate such as cooling or increased precipitation was found during this
65 period to explain such a slow down (Melkonian et al., 2014; Ziemen et al., 2016). Further, Melkonian et
66 al. (2014, 2016)'s estimates used as starting elevation measurement the C-Band SRTM DEM acquired
67 in February 2000, the core of winter in Alaska. The C-Band radar signal is known to penetrate into the
68 cold winter snow and firn such that SRTM maps a surface below the real glacier surface which can
69 bias the elevation change measurements (e.g., Berthier et al., 2006; Rignot et al., 2001). Melkonian et
70 al. (2014, 2016) accounted for this penetration by subtracting the simultaneous C-Band and X-Band
71 SRTM DEM, assuming no penetration of the X-Band DEM (Gardelle et al., 2012), the best available
72 correction at the time of their study. However, this strategy is not appropriate given that the X-band
73 penetration depth has recently been recognized to reach several meters (e.g., Dehecq et al., 2016;
74 Round et al., 2017). In this context, the goal of this brief communication is to recalculate the early 21st
75 century geodetic mass balances of the Juneau and Stikine icefields using multi-temporal ASTER
76 DEMs, carefully excluding the SRTM DEM to avoid a likely penetration bias.



77 **2 Data, methods and uncertainties**

78 The data and methodology applied to the JIF and SIF were identical to the ones used in a recent study
79 deriving region-wide glacier mass balance in High Mountain Asia (Brun et al., 2017). The reader is thus
80 referred to the latter study for details. Only the main processing steps are briefly presented here.

81
82 ASTER DEMs were calculated using the open-source Ames Stereo Pipeline (ASP) (Shean et al.,
83 2016) from 3N (nadir) and 3B (backward) images acquired between 2000 and 2016. All images with
84 cloud coverage lower than 80% were selected, resulting in 153 stereo pairs for the JIF and 368 stereo
85 pairs for the SIF. Images intersecting less than 0.5% of the icefield areas were excluded, reducing the
86 number of stereo pairs to 114 for the JIF and 284 for the SIF. Planimetric and altimetric offsets of each
87 ASTER DEM were corrected using the SRTM DEM as a reference. Offsets were determined on stable
88 terrain, masking out glacierized areas using the Randolph Glacier Inventory v5.0 (Pfeffer et al., 2014).
89 The RGI v5.0 glacier outlines for both the JIF and SIF were mapped using imagery from August of
90 2004 and 2005.

91
92 For the JIF only, we also downloaded directly the ASTER DEMs available online from the LPDAAC
93 website (called 14DMO) because they were used in Melkonian et al. (2014, 2016). The goal is to test
94 the sensitivity of the JIF-wide mass balance to the ASTER DEM generation software. 3D coregistration
95 of the 14DMO DEMs was performed using the same steps as the ASP DEMs. Unlike the ASP DEMs,
96 the 14DMO DEMs contain no data gaps, as they are filled by interpolation.

97
98 From the time series of 3D-coregistered ASTER DEMs, the rate of elevation changes (dh/dt in the
99 following) was extracted for each pixel of our study domain in two steps (Berthier et al., 2016). The
100 SRTM DEM was excluded when extracting the final dh/dt . dh/dt were calculated for the entire period
101 (from 2000 to 2016) and also for different sub-periods for the sake of comparability to published mass
102 balance estimates.

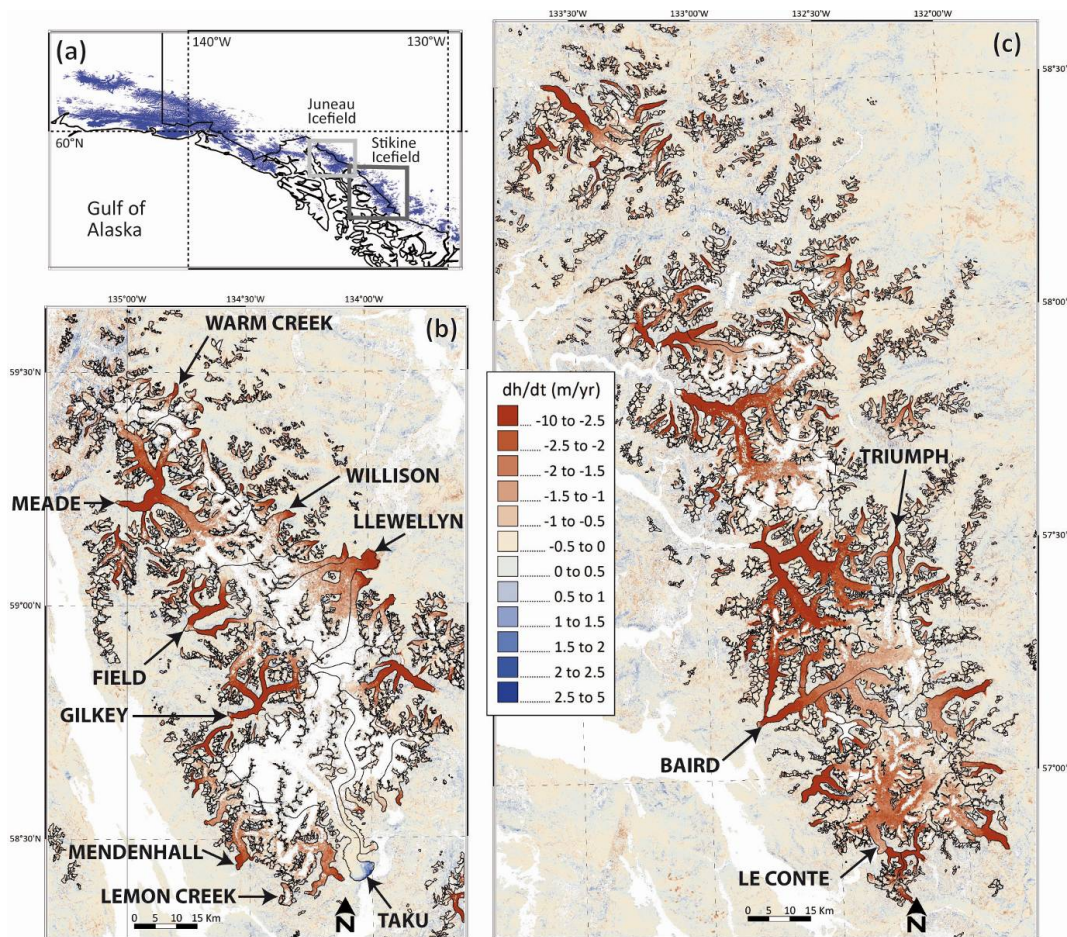
103
104 For both icefields and in each 50-m altitude interval, dh/dt lying outside of ± 3 normalized median
105 absolute deviations (NMAD) were considered as outliers. We further excluded all dh/dt measurements
106 for which the error in the linear fit is larger than 2 m a^{-1} . The total volume change rate was calculated
107 as the integral of the mean dh/dt over the area altitude distribution. The icefield-wide mass balance
108 was obtained using a volume-to-mass conversion factor of $850 \pm 60 \text{ kg m}^{-3}$ (Huss, 2013). The same
109 procedure was followed to compute the glacier-wide mass balances of selected individual glaciers for
110 which mass balances were estimated from repeat laser altimetry surveys (Larsen et al., 2015).

111
112 Uncertainties for dh/dt were computed using the tile method as in Berthier et al. (2016). Splitting the
113 off-glacier terrain in 4 by 4 tiles, we found uncertainties of 0.03 m a^{-1} for JIF and 0.04 m a^{-1} for SIF from
114 2000 to 2016. When data gaps occurred in the dh/dt map, we conservatively multiplied these
115 uncertainties by a factor of five.



116 **3 Results**

117 Rate of elevation changes for the two icefields from 2000 to 2016 are mapped in Figure 1. Most
 118 glaciers thinned rapidly in their lower parts and experienced limited elevation change in their upper
 119 reaches. Thinning rates as negative as 9 m a^{-1} are observed. Taku Glacier (south of the JIF) is an
 120 exception with thickening of up to 4 m a^{-1} at its glacier front.
 121



122
 123 **Figure 1:** Rate of elevation changes for the Juneau and Stikine icefields from 2000 to 2016. (a) Location of the two icefields in
 124 southeast Alaska. Rate of elevation changes (dh/dt) for the JIF (b) and (c) for the SIF. Glacier outlines are from RGI v5.0.
 125 Glaciers surveyed by airborne laser altimetry are labelled. The horizontal scale and the color code are the same for the two
 126 maps. Areas in white correspond to data gaps.

127
 128 The 2000-2016 mass balances are clearly negative for both icefields at $-0.68 \pm 0.15 \text{ m w.e. a}^{-1}$ for JIF
 129 (59% coverage with valid data) and $-0.83 \pm 0.12 \text{ m w.e. a}^{-1}$ for SIF (81% coverage with valid data). If we
 130 apply the linear regression analysis to a subset of the ASTER DEMs to match the time periods studied
 131 by Melkonian et al. (2014, 2016), the icefield-wide mass balances remain mostly unchanged: $-$
 132 $0.64 \pm 0.14 \text{ m w.e. a}^{-1}$ for JIF from 2000 to 2013, 44% coverage with valid data; $-0.78 \pm 0.17 \text{ m w.e. a}^{-1}$ for



133 SIF from 2000 to 2014, 55% coverage with valid data. Our values are $0.51 \text{ m w.e. a}^{-1}$ (JIF) and 0.21 m
134 w.e. a^{-1} (SIF) more negative than in Melkonian et al. (2014, 2016) and statistically different for the JIF.

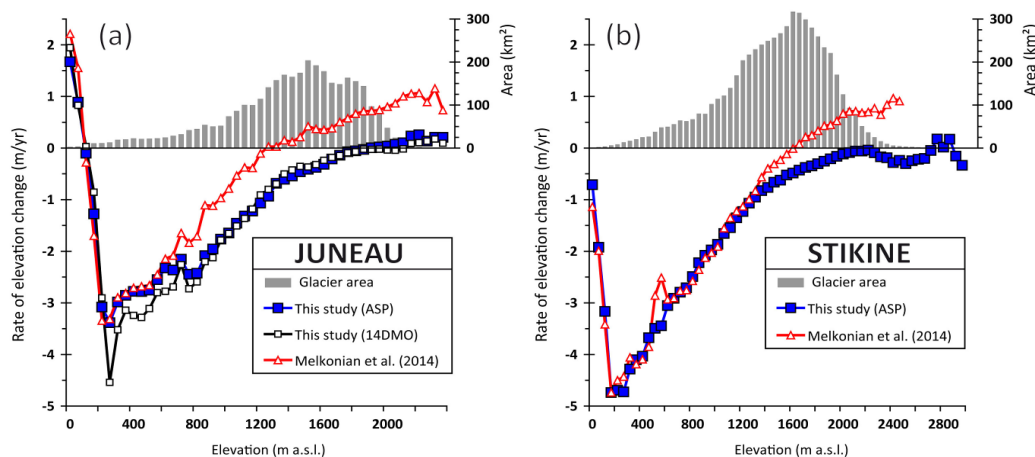
135

136 The coverage with valid dh/dt data drops rapidly for both icefields when shorter time periods are
137 considered. For example, the percentage of valid data is reduced to 8% (respectively 25%) only on the
138 JIF when the 2000-2008 (respectively 2008-2016) period is analyzed. Thus, the ASTER multi-temporal
139 analysis is not appropriate to measure mass balance over periods shorter than 10 years for these two
140 Alaskan icefields. This is due to the presence of many cloudy images and, for cloud-free scenes, to a
141 large percentage of data gaps in individual ASTER DEMs over the accumulation areas of the icefields,
142 a direct result of the limited contrast in the ASTER stereo-images over textureless snow fields.

143

144 In Figure 2, dh/dt are plotted as a function of altitude and compared to the values in Melkonian et al.
145 (2014, 2016). To enable a more direct comparison, we applied the same criteria to average their dh/dt
146 in 50-m altitude bands and exclude outliers. We also considered the same periods, from 2000 to 2013
147 for the JIF and from 2000 to 2014 for the SIF. In the case of the SIF (Figure 2b), we also added the
148 dh/dt obtained by applying our method to the 14DMO DEMs.

149



150

151 **Figure 2:** Rates of elevation change vs. elevation for the JIF from 2000 to 2013 (a) and for the SIF from 2000 to 2014 (b).
152 Results from this study are compared to the dh/dt values obtained in two earlier studies using a similar method (Melkonian et
153 al., 2014, 2016). The grey histograms show the area-altitude distribution.

154

155 For the JIF, an excellent agreement is found between the dh/dt values obtained in this study using the
156 ASP and 14DMO DEMs, except maybe between 250 and 600 m a.s.l. (5% of the icefield area) where
157 the thinning rates are about 0.5 m a^{-1} more negative using the 14DMO DEMs. The area-weighted
158 mean absolute difference between these two curves (ASP and 14DMO) is 0.09 m a^{-1} . The Melkonian
159 et al. (2014) dh/dt generally agree with ours below 600 m a.s.l. Above this elevation, their values are
160 systematically more positive. The difference reaches 0.7 m a^{-1} at 800 m a.s.l. and then remains more



161 or less stable, around $0.7\text{--}0.9\text{ m a}^{-1}$. Melkonian et al. (2014) data suggests thickening of the areas
162 above 1350 m a.s.l. where 62% of the JIF area is located.

163

164 For SIF, a good agreement is found between ours and Melkonian et al. (2016)'s dh/dt below an
165 elevation of 1300 m a.s.l. Above 1300 m the two curves diverge. Our dh/dt are becoming less negative
166 until 2100 m a.s.l. where they become indistinguishable from 0 m a^{-1} up to the SIF highest elevation
167 band. Conversely, in the Melkonian et al. (2016) dataset, dh/dt increases rapidly, crossing 0 m a^{-1} at
168 $\sim 1650\text{ m a.s.l.}$, finally arriving at a thickening rate of $> 0.7\text{ m a}^{-1}$ above 2000 m a.s.l. Thus the
169 difference in SIF-wide mass balance between the two dataset is due to difference in dh/dt above 1300
170 m a.s.l., where 66% of the SIF icefield area is found.

171

172 Comparison of our dh/dt estimates to the ones derived from repeat laser altimetry data is not
173 straightforward because the survey periods differ. For example, for the JIF, six out of nine glaciers
174 were sampled for the first time in 2007. In most cases, it would be technically possible to use a
175 temporal subset of the ASTER DEMs to match the time period of altimetry surveys but, as said above,
176 this would be at the cost of the coverage in our dh/dt maps and would lead to much more uncertain
177 mass balance estimates. Consequently, we preferred to extract dh/dt and the individual glacier mass
178 balance for the longest available time period in the ASTER series (from 2000 to 2016) in order to
179 maximize coverage and thus minimize uncertainties. The pattern of dh/dt with altitude for individual
180 glaciers is in broad agreement between laser altimetry and our ASTER-based results (Supplementary
181 Figure S1). Importantly, for both dataset, no clear thickening was observed in the accumulation areas
182 of glaciers. When individual elevation bins of 50 m are considered, averaged differences between dh/dt
183 from laser altimetry and the ASTER DEMs are typically $0.2\text{ to }0.3\text{ m a}^{-1}$ for individual glaciers. This
184 level of error is similar to the one found previously for the ASTER method in the Mont-Blanc area
185 (Berthier et al., 2016). Glacier-wide mass balances for individual glaciers match well (Table 1).

186

187 The mean mass balance of these 12 glaciers is nearly the same (-0.73 and $-0.74\text{ m w.e. a}^{-1}$) using the
188 two techniques. The standard deviation of the mass balance difference is $0.18\text{ m w.e. a}^{-1}$ ($n=12$). For
189 60 individual glaciers larger than 2 km^2 in High Mountain Asia, Brun et al. (2017) also found a standard
190 deviation of $0.17\text{ m w.e. a}^{-1}$ between the ASTER-based and published glacier-wide mass balance
191 estimates. In the very different geographic context of large maritime glaciers of southeast Alaska, we
192 confirm here their uncertainty estimate for individual glaciers in High Mountain Asia.

193

194 Our results are also in good agreement with field (glaciological) measurements on Taku Glacier. Pelto
195 et al. (2013) found a mass balance of $-0.01\text{ m w.e. a}^{-1}$ between September 2000 and September 2011.
196 We derived the same mass balance ($-0.01 \pm 0.16\text{ m w.e. a}^{-1}$) from ASTER DEMs acquired between
197 2000 and 2016. Conversely, Melkonian et al. (2014)'s mass balance for Taku Glacier was strongly
198 positive at $+0.44 \pm 0.15\text{ m w.e. a}^{-1}$.

199



200 **Table 1.** Glacier-wide mass balances (B_a) of 12 individual glaciers of the JIF and SIF derived from airborne laser
 201 altimetry for different periods (Larsen et al., 2015) and calculated in this study using ASTER DEMs from 2000 to
 202 2016.

Icefield/Glacier	Area km ²	Laser period	B_a Laser m w.e. a ⁻¹ (Larsen et al., 2015)	B_a ASTER m w.e. a ⁻¹ (this study)
Juneau	3398			-0.68
Field	187	2007-2012	-0.94	-0.93
Gilkey	223	2007-2012	-0.75	-0.99
Lemon Creek	9	1993-2012	-0.91	-0.78
Llewellyn	435	2007-2012	-0.61	-0.70
Meade	446	2007-2012	-1.03	-0.88
Mendenhall	106	1999-2012	-0.57	-0.73
Taku	711	1993-2012	0.13	-0.01
Warm Creek	39	2007-2012	-0.67	-0.71
Willison	79	2007-2012	-0.51	-0.69
Sum/Mean glaciers	9		-0.65	-0.71
Stikine	5805			-0.83
LeConte	56	1996-2013	-0.98	-0.93
Baird	435	1996-2013	-0.71	-0.70
Triumph	356	1996-2013	-1.19	-0.86
Sum/Mean glaciers	3		-0.96	-0.83
Mean all Glaciers	12		-0.73	-0.74

203

204 **4 Discussion**

205 We find an excellent agreement between repeat laser altimetry survey and our multi-temporal analysis
 206 of ASTER DEMs both in term of mass balances and pattern of dh/dt with altitude for the JIF and SIF
 207 since 2000 (Supplementary Figure S1). Our results also suggest that the limited number of glaciers
 208 sampled using laser altimetry are representative of the icefields as a whole. This is rather expected for
 209 the JIF because 9 glaciers covering a large fraction of the icefield (66%) were monitored using airborne
 210 data but not straightforward for the SIF where only 3 glaciers, accounting for 15% of the total icefield
 211 area, were surveyed.

212



213 This agreement between our ASTER results and airborne laser altimetry, together with the fact that
214 most studies point toward steady or accelerating mass losses in southeast Alaska (see introduction),
215 suggest that the mass balance is overestimated in Melkonian et al. (2014, 2016). There are two main
216 differences between Melkonian et al. (2014, 2016)'s method and ours that could explain these
217 contending mass balances: (i) they did not generate the DEM themselves but directly download the
218 14DMO product from the LPDAAC website and (ii) they used the SRTM DEM as a starting elevation in
219 their regression analysis to compute dh/dt .

220

221 To test the sensitivity of our results to the ASTER DEM generation software, we applied our processing
222 chain (in particular, excluding the SRTM DEM to infer the final dh/dt) to the 14DMO DEMs. From 2000
223 to 2016, we found a JIF-wide mass balance of -0.67 ± 0.27 m w.e. a^{-1} , in striking agreement with the
224 value derived from ASP DEMs (-0.68 ± 0.15 m w.e. a^{-1}). The pattern of dh/dt with elevation is also in
225 excellent agreement (Figure 2a). Uncertainties are nearly doubled when applying our method to the
226 14DMO DEMs: this is explained by larger errors of dh/dt off glacier (0.06 m a^{-1} for 14DMO DEMs vs.
227 0.03 m a^{-1} for ASP DEMs) and a lower coverage of the JIF with valid dh/dt data (49% for 14DMO
228 DEMs vs. 59% for ASP DEMs). The latter may appear counter-intuitive as the 14DMO DEMs are
229 delivered with no data gaps. The larger percentage of data gaps in the final 14DMO dh/dt maps results
230 from the higher noise level of the individual 14DMO DEMs and demonstrate the efficiency of our filters
231 to exclude unreliable dh/dt values.

232

233 Thus, we conclude that a likely explanation why Melkonian et al. (2014, 2016) found too positive mass
234 balance for the JIF and, to a lesser extent, for the SIF is associated with the SRTM DEM and in
235 particular the penetration of the C-Band radar signal into cold winter snow and firn. This interpretation
236 is further supported by the fact that dh/dt curves nicely agree in the ablation areas where SRTM
237 penetration depth is negligible and diverge in the accumulation areas where the largest penetration
238 depths are expected (Figure 2). As noted in the introduction, Melkonian et al. (2014, 2016) attempted
239 to account for this by subtracting the C-Band and X-Band SRTM DEM, assuming no penetration of the
240 X-Band DEM (Gardelle et al., 2012). However, studies have measured X-band penetration depth of
241 several meters (e.g., Dehecq et al., 2016; Round et al., 2017). In the case of the SIF, Melkonian et al.
242 (2016) assumed no penetration below 1000 m a.s.l. and 2 m for elevations above 1000 m. Aware of
243 how uncertain this correction was, these authors also proposed (their supplementary material section
244 6.3 and, Table S4) a different correction with no penetration below 1000 m a.s.l. and a linear increase
245 from 2 to 8 m from 1000-2500 m a.s.l. Using this alternative scenario, they found an icefield-wide mass
246 balance of -0.85 m w.e. a^{-1} , in better agreement with our value of -0.78 ± 0.17 m w.e. a^{-1} from 2000 to
247 2014. Their 2 to 8 m penetration depth is consistent with the penetration gradient we inferred here by
248 subtracting the SRTM DEM from a reconstructed DEM, obtained by extrapolating dh/dt to the time of
249 acquisition of the SRTM as proposed in Wang and Käab (2015). This is also consistent with a first-
250 order estimate of the penetration depth inferred from the elevation difference between the SRTM DEM
251 and laser altimetry profiles acquired in late August 1999 and May 2000 over Baird and Taku glaciers.



252 However, the latter estimates should be considered with care considering the complexity to account for
253 seasonal elevation changes, long term elevation changes and the difficulty to estimate the vertical
254 offset between the two elevation dataset on ice-free terrain.

255

256 The fact that the positive bias in Melkonian et al. (2014, 2016) mass balances was larger for the JIF
257 and than for the SIF suggests a larger SRTM penetration depth for the JIF. It indicates that the
258 penetration is probably spatially variable (depending on the firm conditions in February 2000) such that
259 a correction determined on a single icefield (or worse a single glacier) may not apply to neighbouring
260 glacier areas.

261

262 Larsen et al. (2007) used the SRTM DEM as their final topography after applying a linear correction of
263 SRTM with altitude (2.6 m per 1000 m elevation, with a -2.5 offset at 0 elevation) determined by
264 comparing SRTM to August 2000 laser altimetry data. Such a correction would correspond to a
265 maximum SRTM penetration of ~1.5-2 m above 1500 m a.s.l. much smaller than what we found here.
266 Thus, the fact that SRTM penetration depth is larger than previously thought over southeast Alaska
267 icefields may also explain why Larsen et al. (2007) found larger mass losses than Arendt et al. (2002)
268 and Berthier et al. (2010) who both used only non-penetrating optical (Lidar or stereo-imagery) data.

269

270 An uneven seasonal distribution of the ASTER DEMs could bias the multi-annual mass balances
271 derived using the ASTER method is linked to the (Berthier et al., 2016). This is especially crucial in
272 maritime environment such as southeast Alaska where large seasonal height variations are expected.
273 As in the case of the Mont-Blanc area (Figure 6 in Berthier et al., 2016), we sampled an hypothetical
274 seasonal cycle in surface elevation changes at the time of acquisition of all ASTER DEMs over the JIF
275 and fitted a linear regression to the elevation change time series. Assuming a seasonal amplitude as
276 large as 10 m, the slope of the regression line is very close to 0 (-0.007 m a^{-1}) suggesting no seasonal
277 bias in the dates of the ASTER DEMs. To confirm the lack of seasonal bias and because the majority
278 of the ASTER images were acquired close to accumulation peak, we also calculated a mass balance
279 for the JIF considering only the 61 ASTER DEMs acquired in March, April and May between 2000 and
280 2016. For this alternative mass balance estimate, the coverage with valid data is reduced to 38%. At -
281 $0.58 \pm 0.18 \text{ m w.e. a}^{-1}$, the JIF-wide mass balance is slightly less negative but not statistically different
282 from the "all seasons" value ($-0.68 \pm 0.15 \text{ m w.e. a}^{-1}$, 59% of valid data). The pattern of dh/dt with
283 altitude is also very similar.

284

285 **5 Conclusion**

286 In this study, we show that the Juneau and Stikine icefields continued to lose mass rapidly from 2000
287 to 2016. The mass balances from repeat airborne laser altimetry and multi-temporal ASTER DEMs are
288 reconciled if the SRTM DEM is discarded when extracting the rate of elevation change on glaciers from
289 the elevation time series. Multi-temporal analysis of DEMs derived from satellite optical stereo-imagery



290 is thus a powerful method to estimate geodetic region-wide mass balances over time intervals of,
291 typically, more than 10 years. The strength of the ASTER method lies in the fact that it is based on an
292 homogeneous and continuous archive of imagery built since 2000 using the same sensor. Maintaining
293 openly available medium- to high-resolution stereo capabilities should be a high priority among space
294 agencies in the future.

295

296 Previously published mass balances for these Alaska icefields using SRTM and ASTER DEMs were
297 likely biased positively because of the strong penetration of the C-Band and X-Band radar signal into
298 the cold winter snow and firn in February, when the SRTM was flown. Accounting for this penetration
299 by subtracting the C-Band and X-Band SRTM DEMs (as often done before) is not appropriate because
300 the X-Band penetration depth can reach several meters. Caution should thus be used when deriving
301 mass balance using SRTM and Tandem-X DEMs over time period of less than ~20 years. Comparing
302 DEMs acquired at the same time of the year using the same radar wavelength (e.g., Neckel et al.,
303 2013) is one promising strategy to limit the bias due to differential radar penetration.

304 **Acknowledgements**

305 We thank Fanny Brun for sharing her python codes. We thank the Global Land Ice Measurement from
306 Space (GLIMS) project that allowed the population of a vast archive of ASTER stereo images over
307 glaciers. E.B. acknowledges support from the French Space Agency (CNES) and the Programme
308 National de Télédétection Spatiale grant PNTS-2016-01.

309 **Author contributions**

310 E.B. designed the study, made the data analysis and lead the writing. C.L. provided the laser altimetry
311 data. W.D., M.W. and M.P. provided unpublished results. All authors discussed the results and wrote
312 the paper.

313 **References**

314 Arendt, A., Luthcke, S., Gardner, A., O'Neel, S., Hill, D., Moholdt, G. and Abdalati, W.: Analysis of a GRACE
315 global mascon solution for Gulf of Alaska glaciers, *Journal of Glaciology*, 59(217), 913–924,
316 doi:10.3189/2013JoG12J197, 2013.

317 Arendt, A. A., Echelmeyer, K. A., Harrison, W. D., Lingle, C. S. and Valentine, V. B.: Rapid wastage of Alaska
318 glaciers and their contribution to rising sea level, *Science*, 297(5580), 382–386, 2002.

319 Berthier, E., Arnaud, Y., Vincent, C. and Remy, F.: Biases of SRTM in high-mountain areas: Implications for the
320 monitoring of glacier volume changes, *Geophysical Research Letters*, 33(8), L08502,
321 doi:10.1029/2006GL025862, 2006.

322 Berthier, E., Schiefer, E., Clarke, G. K. C., Menounos, B. and Rémy, F.: Contribution of Alaskan glaciers to sea-
323 level rise derived from satellite imagery, *Nat Geosci*, 3(2), 92–95, doi:10.1038/ngeo737, 2010.



- 324 Berthier, E., Cabot, V., Vincent, C. and Six, D.: Decadal region-wide and glacier-wide mass balances derived
325 from multi-temporal ASTER satellite digital elevation models. Validation over the Mont-Blanc area, *Frontiers in*
326 *Earth Science*, 4, doi:10.3389/feart.2016.00063, 2016.
- 327 Brun, F., Berthier, E., Wagnon, P., Kaab, A. and Treichler, D.: A spatially resolved estimate of High Mountain
328 Asia glacier mass balances from 2000 to 2016, *Nature Geoscience*, 10(9), 668–673, doi:10.1038/ngeo2999,
329 2017.
- 330 Dehecq, A., Millan, R., Berthier, E., Gourmelen, N. and Trouve, E.: Elevation changes inferred from TanDEM-X
331 data over the Mont-Blanc area: Impact of the X-band interferometric bias, *IEEE Journal of Selected Topics in*
332 *Applied Earth Observations and Remote Sensing*, 9(8), 3870–3882, doi:10.1109/JSTARS.2016.2581482, 2016.
- 333 Gardelle, J., Berthier, E. and Arnaud, Y.: Impact of resolution and radar penetration on glacier elevation changes
334 computed from multi-temporal DEMs, *Journal of Glaciology*, 58(208), 419–422, 2012.
- 335 Huss, M.: Density assumptions for converting geodetic glacier volume change to mass change, *The Cryosphere*,
336 7(3), 877–887, doi:10.5194/tc-7-877-2013, 2013.
- 337 Kienholz, C., Herreid, S., Rich, J. L., Arendt, A. A., Hock, R. and Burgess, E. W.: Derivation and analysis of a
338 complete modern-date glacier inventory for Alaska and northwest Canada, *Journal of Glaciology*, 61(227), 403–
339 420, doi:10.3189/2015JoG14J230, 2015.
- 340 Larsen, C. F., Motyka, R. J., Arendt, A. A., Echelmeyer, K. A. and Geissler, P. E.: Glacier changes in southeast
341 Alaska and northwest British Columbia and contribution to sea level rise, *J Geophys Res-Earth*, 112(F1), F01007,
342 doi:10.1029/2006JF000586, 2007.
- 343 Larsen, C. F., Burgess, E., Arendt, A. A., O’Neel, S., Johnson, A. J. and Kienholz, C.: Surface melt dominates
344 Alaska glacier mass balance, *Geophysical Research Letters*, 42(14), 5902–5908, doi:10.1002/2015GL064349,
345 2015.
- 346 Melkonian, A. K., Willis, M. J. and Pritchard, M. E.: Satellite-derived volume loss rates and glacier speeds for the
347 Juneau Icefield, Alaska, *Journal of Glaciology*, 60(222), 743–760, doi:10.3189/2014JoG13J181, 2014.
- 348 Melkonian, A. K., Willis, M. J. and Pritchard, M. E.: Stikine Icefield Mass Loss between 2000 and 2013/2014,
349 *Frontiers in Earth Science*, 4, 89, doi:10.3389/feart.2016.00089, 2016.
- 350 Neckel, N., Braun, A., Kropáček, J. and Hochschild, V.: Recent mass balance of the Purogangri Ice Cap, central
351 Tibetan Plateau, by means of differential X-band SAR interferometry, *The Cryosphere*, 7(5), 1623–1633,
352 doi:10.5194/tc-7-1623-2013, 2013.
- 353 Pelto, M., Kavanaugh, J. and McNeil, C.: Juneau Icefield Mass Balance Program 1946–2011, *Earth Syst. Sci.*
354 *Data*, 5(2), 319–330, doi:10.5194/essd-5-319-2013, 2013.
- 355 Pfeffer, W. T., Arendt, A. A., Bliss, A., Bolch, T., Cogley, J. G., Gardner, A. S., Hagen, J.-O., Hock, R., Kaser, G.,
356 Kienholz, C., Miles, E. S., Moholdt, G., Moelg, N., Paul, F., Radic, V., Rastner, P., Raup, B. H., Rich, J., Sharp,
357 M. J., Andeassen, L. M., Bajracharya, S., Barrand, N. E., Beedle, M. J., Berthier, E., Bhambri, R., Brown, I.,
358 Burgess, D. O., Burgess, E. W., Cawkwell, F., Chinn, T., Copland, L., Cullen, N. J., Davies, B., De Angelis, H.,
359 Fountain, A. G., Frey, H., Giffen, B. A., Glasser, N. F., Gurney, S. D., Hagg, W., Hall, D. K., Haritashya, U. K.,
360 Hartmann, G., Herreid, S., Howat, I., Jiskoot, H., Khromova, T. E., Klein, A., Kohler, J., König, M., Kriegel, D.,
361 Kutuzov, S., Lavrentiev, I., Le Bris, R., Li, X., Manley, W. F., Mayer, C., Menounos, B., Mercer, A., Mool, P.,
362 Negrete, A., Nosenko, G., Nuth, C., Osmonov, A., Pettersson, R., Racoviteanu, A., Ranzi, R., Sarikaya, M. A.,
363 Schneider, C., Sigurdsson, O., Sirguey, P., Stokes, C. R., Wheate, R., Wolken, G. J., Wu, L. Z. and Wyatt, F. R.:
364 The Randolph Glacier Inventory: a globally complete inventory of glaciers, *Journal of Glaciology*, 60(221), 537–
365 552, doi:10.3189/2014JoG13J176, 2014.
- 366 Rignot, E., Echelmeyer, K. and Krabill, W.: Penetration depth of interferometric synthetic-aperture radar signals in
367 snow and ice, *Geophysical Research Letters*, 28(18), 3501–3504, 2001.
- 368 Round, V., Leinss, S., Huss, M., Haemmig, C. and Hajsek, I.: Surge dynamics and lake outbursts of Kyagar
369 Glacier, Karakoram, *The Cryosphere*, 11(2), 723–739, doi:10.5194/tc-11-723-2017, 2017.
- 370 Shean, D. E., Alexandrov, O., Moratto, Z. M., Smith, B. E., Joughin, I. R., Porter, C. and Morin, P.: An automated,
371 open-source pipeline for mass production of digital elevation models (DEMs) from very-high-resolution



- 372 commercial stereo satellite imagery, ISPRS Journal of Photogrammetry and Remote Sensing, 116, 101–117,
373 doi:10.1016/j.isprsjprs.2016.03.012, 2016.
- 374 Wang, D. and Kääh, A.: Modeling Glacier Elevation Change from DEM Time Series, Remote Sensing, 7(8),
375 10117, 2015.
- 376 Ziemen, F. A., Hock, R., Aschwanden, A., Khroulev, C., Kienholz, C., Melkonian, A. and Zhang, J.: Modeling the
377 evolution of the Juneau Icefield between 1971 and 2100 using the Parallel Ice Sheet Model (PISM), Journal of
378 Glaciology, 62(231), 199–214, doi:10.1017/jog.2016.13, 2016.